Submitted as a "Communication" to *ChemElectroChem*, Revised October 2018

Li_3BN_2 as a Transition Metal Free, High Capacity Cathode for Li-ion Batteries

Satyanarayana Emani [a,b], Caihong Liu [a,b], Maziar Ashuri [a,b], Karan Sahni [a,b], Jinpeng Wu [c,d], Wanli Yang [d], Karoly Németh [e,*], Leon L. Shaw [a,b,*]

[a] Department of Mechanical, Materials and Aerospace Engineering, Illinois Institute of Technology, Chicago, IL, USA
[b] Wanger Institute for Sustainable Energy Research (WISER), Illinois Institute of Technology, Chicago, IL, USA
[c] Geballe Laboratory for Advanced Materials, Stanford University, Stanford, California 94305, USA
[d] Advanced Light Source, Lawrence Berkeley National Laboratory, Berkeley, California 94720, USA
[e] Department of Physics, Illinois Institute of Technology, Chicago, IL, USA

Keywords: Li_3BN_2; Cathodes; Transition metal free electrodes; Li-ion batteries;

Corresponding authors:
K. Németh, nemeth@agni.phys.iit.edu; Tel: +1-630-632-2382
L. Shaw, lshaw2@iit.edu; Tel: +1-312-567-3844

Li_3BN_2 is investigated for the first time as a transition metal free, high capacity cathode material for Li-ion batteries. It is shown that α-Li_3BN_2 can exhibit a specific capacity of 890 mAh/g with the charge storage mechanism associated with the valence state change of N ions in the BN_2 anion. The specific capacity demonstrated in this study is the highest one ever reported in literature for an intercalation-type cathode material. Further, using the valence state change of N ions as a charge storage mechanism opens the door for designing additional high performance, transition metal free electrodes in the future.

Li-ion batteries (LIBs) have revolutionized portable electronic devices in the past three decades, and have the potential to make great impact on vehicle electrification.[1-3] In spite of their eminent potential, the state-of-the-art LIBs have not been able to meet the need for vehicle electrification, which requires both high energy density and high power density simultaneously.[4] To increase the energy density, current research in the cathode is aimed at developing materials with higher capacities or higher operating voltages.[1-3, 5] In this regard, high-voltage doped $LiMn_2O_4$ has been studied extensively.[5-7] However, doped $LiMn_2O_4$ only exhibits a limited capacity of ~130 mAh/g.[1] In contrast, lithium-rich layered oxides, $Li[Li,Mn,Ni,Co]O_2$, deliver high capacities of ~250 mAh/g when charged above 4.5 V,[6, 8-9] but they have inferior rate capacity and a large first cycle irreversible capacity loss.[6] Lithium- and manganese-rich nickel-manganese-cobalt (LMR-NMC) layered composite oxides show high charge/discharge capacity (> 240 mAh/g), but suffer from voltage fade.[10-11] To increase the energy density beyond what the redox of cationic species can offer, oxygen redox in intercalation oxides has been explored.[12-14] Furthermore, non-intercalation materials such as S and Li_2S cathodes have

also been studied.[15-19] These S-based cathode materials have very high theoretical capacities (>1,000 mAh/g), but suffer from large volume change (~80%), polysulfide dissolution and insulating problems, leading to poor cycling life and low capacity retention.[15-19] As such, new types of cathode materials with high capacities and high energy densities are urgently needed to meet the need for vehicle electrification.

In this study, we have investigated a completely new class of cathode materials that eliminate the need of using transition metals as they are built from light elements only, such as B, N and C. Recent studies through density functional theory (DFT) calculations have predicted a new class of cathode materials based on functionalized hexagonal boron nitride (FBN) materials.[20-22] The DFT calculations reveal that functionalization of boron nitrides can tune the electrochemical potentials of FBN materials and create intercalation-type materials with ultrahigh specific capacities and unprecedented energy densities because of the elimination of heavy transition metals.[20-22] The charge storage mechanism of FBN materials is predicted to be accomplished by redox reactions due to the valence state change of N ions.[20-22] Inspired by these predictions, we have synthesized Li_3BN_2 powder via reaction between Li_3N and h-BN at 900 °C[23] (see Supporting Information for experimental details) and carried out the first-ever electrochemical investigation of Li_3BN_2 (a 3D member of FBN materials that can be derived from Li_3N functionalized 2D h-BN) for its potential as a transition metal free, high-capacity cathode material for Li-ion batteries. We demonstrate that the α-Li_3BN_2 powder obtained from the reaction between Li_3N and h-BN can exhibit an unprecedented specific capacity of 890 mAh/g with the charge storage mechanism associated with the valence state change of N ions in the BN_2 anion during Li-ion intercalation and de-intercalation. The specific capacity of 890 mAh/g demonstrated in this study is the highest specific capacity ever reported in literature for an intercalation-type cathode material. The specific discoveries of this study are described below.

The charge/discharge curves of an α-Li_3BN_2 coin cell with a Li foil as the anode at the 0.1C rate (1C = 890 mA/g) are shown in Figure 1(a). The first operation of the as-synthesized α-Li_3BN_2 in this study is charge, but only exhibits a specific capacity of ~300 mAh/g. However, the first discharge after the first charge has delivered 890 mAh/g capacity, while the specific capacity of the second charge has increased significantly from the previous 300 mAh/g to 840 mAh/g. To ensure that the high carbon black (CB) concentration (45 wt%) used in the electrode did not alter the specific capacity of α-Li_3BN_2 significantly, we have measured charge/discharge curves of pure CB electrodes with a Li foil as the counter electrode. The results from the pure CB half cells indicate that CB only contributes to less than 0.5% of the total storage capacity (see Supporting Information for details). Note that the first discharge capacity of 890 mAh/g from α-Li_3BN_2 is very close to the theoretical capacity (899 mAh/g) based on the following electrochemical reaction predicted from the DFT calculation.[20-22]

$$\alpha\text{-}Li_3BN_2 \Leftrightarrow LiBN_2 + 2Li^+ + 2e^- \qquad (1)$$

It is noted from Figure 1(a) that there are two plateaus in both charge and discharge curves. To understand this phenomenon, cyclic voltammetry (CV) of the α-Li_3BN_2 half cell is conducted. As shown in Figure 1(b),

there are two anodic and two cathodic peaks in the cyclic voltammogram. The first anodic peak is located at ~1.85 V vs. Li/Li^+ and the second anodic peak at ~2.23 V. These two anodic peak positions are very close to the two voltage plateaus during charge, unambiguously indicating that charging of α-Li_3BN_2 proceeds in two oxidation steps. Based on the DFT calculations,[21-22] we hypothesize that the first oxidation corresponds to the valence state change of N ions in the BN_2 anion from 3^- to 2.5^-, whereas the second oxidation is due to the further change of N ions from 2.5^- to 2^-. This hypothesis is consistent with our X-ray photoelectron spectroscopy (XPS) and soft X-ray absorption spectroscopy (sXAS) analyses to be shown later. Similarly, the two cathodic peaks at ~2.10 V and ~1.65 V vs. Li/Li^+ match the two voltage plateaus during discharge very well, clearly revealing that discharging of α-Li_3BN_2 occurs via two reduction steps. Based on the CV curve, the two cathodic peaks can be assigned to the valence state change of N ions in the BN_2 anion from 2^- to 2.5^- for the peak at 2.10 V and from 2.5^- to 3^- for the peak at 1.65 V. The stepwise oxidation of the BN_2^{3-} anion has also been pointed out in the melt-phase N_2/BN_2^{3-} electrode [24] and in thermal decomposition of Na_2KBN_2.[25]

To confirm the redox reactions of α-Li_3BN_2 are indeed due to the valence state change of N ions in the BN_2 anion, we have conducted the XPS analysis of the α-Li_3BN_2 cathode after different states of charge. The states of charge for the α-Li_3BN_2 cathode subjected to XPS analysis are marked in Figure 1(a) as S1 (discharged state), S2 (partially charged state) and S3 (near fully charged state). As shown in Figure 2(a), the N1s spectra of these samples are quite broad and unsymmetric, suggesting overlap of several peaks. Based on the charge/discharge profile (Figure 1) and the resonance structures of the BN_2^{3-} anion and its gradually delithiated versions of Li_2BN_2 and $LiBN_2$ predicted via DFT calculations,[21] 3 major peaks in each N1s spectrum can be fitted and attributed to BN_2^{3-}, BN_2^{2-} and BN_2^{1-} resonant groups. It is known that the N1s spectrum of a substance with covalent bond and/or negative valence state is normally peaked at < 400.0 eV, such as N in h-BN[26-27] and Li_3N.[28-29] N1s located around 398.5 eV or lower indicates the formation of B-N covalent bond sharing 3 pair of electrons.[26-27] Furthermore, the higher the electron cloud density around N atom, the lower the binding energy. Hence, the binding energy sequence from low to high is Li_3N, BN_2^{3-}, BN_2^{2-} and BN_2^{1-}, as assigned in Figure 2(a). Among them, only the binding energy of BN_2^{1-} anion (≥ 399.2 eV) is higher than that of h-BN, which is consistent with their resonant structure and valence state.

Several general trends can be observed from Figure 2(a), while the quantitative fitting results of the N1s peak are summarized in Table S1 of Supporting Information. These trends include: (i) the discharged electrode (S1) has the highest concentration of the BN_2^{3-} anion, (ii) the fully charged electrode (S3) has the highest concentration of the BN_2^{1-} anion, and (iii) the partially charged electrode (S2) has the highest concentration of the BN_2^{2-} anion among the 3 samples. These general trends reveal unambiguously that charge of α-Li_3BN_2 follows the sequence of oxidation and delithiation of Li_3BN_2 to become Li_2BN_2 (partially charged) and then to $LiBN_2$ (fully charged). Thus, the present XPS analysis confirms that the redox reactions of α-Li_3BN_2 are associated with the valence state change of N ions in the BN_2 anion, as predicted from the DFT calculations.[21,22] Three additional features are noted. The first is that BN_2^{3-}, BN_2^{2-} and BN_2^{1-} anions are present in all samples even though their relative concentrations are changed. This is not a surprise since

inhomogeneous charge/discharge is typical because not all the active particles are connected to conductive network and there is non-uniform distribution of the active material.[30-32] The second is the small shift in the binding energy of BN_2^{3-}, BN_2^{2-} and BN_2^{1-} anion peaks (≤ 0.5 eV) from one charge state to another. One likely mechanism for this small shift is that the N1s peak of the BN_2 anion is not from an isolated N-B-N ion; instead, its binding energy may depend to a small extent on the overall Li-site occupancy as well. The third feature noted is the presence of an N1s peak with very low binding energy (~395.2 eV) in the fully charged sample. This peak could be related to Li_3N,[28,29] implying decomposition of Li_3BN_2. Whether this is indeed the case needs additional investigation in the future.

To explore whether α-Li_3BN_2 is a conversion-type or intercalation-type cathode, we have conducted X-ray diffraction (XRD) analysis of the α-Li_3BN_2 cathode after different charge/discharge conditions. The XRD pattern of the as-synthesized α-Li_3BN_2 is shown in Figure 2(b). It is consistent with the α-Li_3BN_2 crystal defined in ICDD PDF card #04-013-9542 and matches the crystal structure of α-Li_3BN_2 derived from the DFT calculations well.[21] The presence of a small amount of the unreacted h-BN and the impurity Li_3TaN_3 is noted. The latter is due to the use of Ta foil during synthesis. Nevertheless, the major phase of the reaction product is α-Li_3BN_2 which has a 1D conjugated chain having -Li-N-B-N- repeating units (Figure 2c). The –N–B–N– part of the –Li–N–B–N– repeating unit is the dinitridoborate anion, BN_2^{3-}, thus each repeating unit –Li–N–B–N– carries two negative charge. The two negative charge of the –Li–N–B–N– repeating unit is counterbalanced by two Li^+ ions per formula unit, located between sheets of the strands. This layered structure strongly resembles layered oxides in LIBs. The Li in the chains is coordinated to 2 nearest N-s, while the Li between the layers is coordinated to 4 nearest N-s.

The XRD patterns of the cathode containing 45 wt% α-Li_3BN_2, 45 wt% carbon black (CB), and 10 wt% PVDF before and after charge and discharge at different states are presented at Figure 2(d). The different states of the cathode for the XRD analysis are marked in Figure 1(a) as X1, X2 and X3. Note that the signal-to-noise ratio in Figure 2(d) is not as good as the one in Figure 2(b) because the XRD pattern in Figure 2(b) is taken without the presence of CB and PVDF. However, the most interesting feature of Figure 2(d) is the similar XRD pattern displayed by all three conditions (X1, X2 and X3) with a new peak at 2θ = ~50.6° emerging for X3. The nature of this new peak remains to be identified in the future, but it may be due to the formation of h-BN because this peak coincides with the third strongest peak of h-BN (ICDD PDF card: 00-034-0421). Note that the formation of h-BN has been detected in the N_2/Li_3BN_2 electrode operating at 550°C as a product of the charging process.[24]

In spite of the similarity of XRD patterns for X1, X2 and X3 conditions, the relative intensities of major peaks are changing with the state of charge. For instance, at the X1 condition the peak intensities are very close to those of α-Li_3BN_2 (ICDD PDF card #04-013-9542). However, after charge (X2) the intensities of (110), (002) and (210) become stronger. After discharge (X3) the intensities of (110) and (002) become weaker, while (210) becomes much stronger. To understand what is responsible for these peak intensity changes, we have performed XRD modeling using “Crystal Maker” software to investigate how the intensity of each peak of α-Li_xBN_2 varies with the Li-ion site occupancy. The modeling results (Figures 2e and 2f) reveal that if delithiation during charge occurs via removal of Li ions between the layers of the linear –Li-N-

B-N- chains, (110), (002) and (210) peaks become gradually stronger with respect to other peaks. This is consistent with the experimental observation, i.e., (110), (002) and (210) peaks all become stronger, when the cell is charged from X1 to X2 (Figure 2d). The modeling also reveals that if delithiation during charge occurs via removal of Li ions in the layers of the linear –Li-N-B-N- chains, the intensities of (110), (002) and (210) peaks change little with respect to other peaks. Clearly, this situation is not what being observed in the experiment. Therefore, it can be concluded that delithiation of α-Li_xBN_2 occurs mainly through the removal of Li ions between the layers of the linear –Li-N-B-N- chains. This experimental observation is in good agreement with the prediction of the DFT calculations.[21-22] Additionally, since Li_3BN_2, Li_2BN_2 and $LiBN_2$ at different states of charge have the same crystal structure but different Li occupancies as the XRD pattern of α-Li_3BN_2 (ICDD PDF card #04-013-9542), one can conclude that the as-synthesized lithium boron nitride is a Li-deficient compound, α-$Li_{3-x}BN_2$ ($x > 0$) because the first charge capacity is only ~300 mAh/g and its open circuit voltage is between fully charged and discharged states (Figure 1a).

Although XPS analysis has revealed that charge and discharge of α-Li_3BN_2 correspond to oxidation and reduction of N ions in the BN_2 anion respectively, XPS is a surface-sensitive technique. Thus, to probe the oxidation state of N in bulk-Li_3BN_2 during charge/discharge, synchrotron-based photon-in-photon-out sXAS of the N-K edge has been conducted on several key samples. Such sXAS experiments through the fluorescence mode have the probe depth of ~100 nm, thus serving as a good complementary to the XPS analysis. As shown in Figure 3(a), there are three evolving features of the N-K XAS results, at ~399.5, ~401.0 and ~403.0 eV, upon cycling. We note that the photon energy differences between these N-K XAS features are consistent with those obtained from the XPS analysis, i.e., ~2.0 eV (vs. ~1.7 eV for XPS) between the high energy features and ~1.5 eV (vs. ~1.3 eV for XPS) between the low energy features. Considering XPS probes the core level states, while XAS measures the conduction band states that could be slightly renormalized with the existence of the core hole, such a comparison shows a great consistency between the XPS and XAS results, and the three features, from low to high energies, are naturally assigned to the BN_2^{3-}, BN_2^{2-} and BN_2^{1-} anions, respectively. Furthermore, the evolution of the three features upon cycling is consistent with the XPS result. Specifically, two clear trends are observed, that is, (i) the BN_2^{1-} peak becomes stronger after charge because BN_2^{3-} and BN_2^{2-} anions get oxidized, and (ii) both BN_2^{1-} and BN_2^{2-} peaks become weaker after discharge because BN_2^{1-} and BN_2^{2-} anions are reduced to become the BN_2^{3-} anion. As mentioned before, the presence of all three BN_2 anions in one sample is due to inhomogeneous charge/discharge in the electrode.[30-32] Thus, the sXAS and XPS analyses are consistent in both the relative energy positions and the evolution of the lineshape, indicating that both the surface and bulk of α-Li_3BN_2 have the same redox mechanisms.

It is interesting to note that the sXAS analysis reveals that the as-synthesized lithium boron nitride powder is dominated by BN_2^{3-} and BN_2^{2-} anions in the bulk, consistent with the previous conclusion that the as-synthesized lithium boron nitride is a Li-deficient compound, i.e., it is α-$Li_{3-x}BN_2$ ($x > 0$). Thus, there are Li vacancies in the as-synthesized condition. Furthermore, it is reasonable to assume that there is random filling of the two different Li positions (in and between the -Li-N-B-N- chains) due to the high synthesis temperature

and relatively quick cooling of the system after synthesis. This as-synthesized condition provides a possible mechanism for the observed phenomenon that the first cycle shows a charge plateau at a lower potential than the second cycle (Figure 1a), as discussed below. After the first discharge, all Li positions are filled and the subsequent delithiation in the charge process primarily vacates Li ions between the layers of the -Li-N-B-N- chains, as revealed from the evolution of XRD patterns (see Figures 2d, 2e and 2f), and leaves the chains largely intact. Although the net result of delithiation is the extraction of Li^+ ions between the layers of the -Li-N-B-N- chains, the delithiation pathway entails extraction of a Li^+ ion in the -Li-N-B-N- chain first and then this vacancy is filled by a Li^+ ion between the chains.[21] In other words, delithiation proceeds via migration of Li^+ ions from between the chains through the in-chain positions toward the surface of the crystal where they leave the crystal. Ultimately, all Li ions between the chains will be vacated and only in-chain Li positions will remain filled, just as the XRD data indicates. As such, the electrochemical potential for delithiation corresponds to the binding energy of Li in the chains and not to the binding energy of Li between the chains. The longer the chains, the greater the binding energy of Li in the chains due to the presence of long range conjugated pi-electron systems along the chains.[21] Since the chains were fragmented in the as-synthesized material, the binding energy of Li in them was smaller than after the first discharge when the chains were fully established. This binding energy difference is indicated by the difference in the voltage plateaus of the first and second charges, i.e., Li extraction happens at an increased voltage in the second charge, due to the presence of the longer -Li-N-B-N- chains.

The charge/discharge cycle stability of α-Li_3BN_2 has also been evaluated. It is found that the capacity decay over cycles is relatively fast and depends on the solvent used to prepare the cathode slurry and the electrolyte. As shown in Figure 3(b), the capacity retention of α-Li_3BN_2 is the best if N-methyl-2-pyrrolidone (NMP) is used to prepare both the cathode slurry and the electrolyte, but the cathode prepared using tetraethylene glycol dimethyl ether (tetraglyme) as the solvent for the slurry and NMP as the solvent for the electrolyte has the highest specific capacity in the first discharge. In all cases, the two charge/discharge plateaus are still present after 30 and 50 cycles (Figures 3c, 3d and S1), indicating that two-electron-transfer redox reactions still operate after 30 to 50 cycles even though the specific capacity has decreased significantly. The electrodes made using NMP for slurry preparation and tetraglyme or ethylene carbonate + diethyl carbonate (EC + DEC) as the electrolyte have also been evaluated, but did not result in good specific capacity (Figure S2). The phenomenon of fast capacity decay is not fully understood yet, but may suggest the wettability issue of α-Li_3BN_2 by the solvent or possible side reactions between the solvent and α-Li_3BN_2. Thus, future research in this area is warranted and proper coatings may offer a solution to the capacity decay problem if the decay is due to side reactions. Note that Li_3N, a compound related to Li_3BN_2, has been reported to be incompatible with NMP due to the high reactivity of Li_3N.[29,33] However, this problem can be addressed by surface passivation through a dense layer consisting of crystalline Li_2O and Li_2CO_3.[29] Despite of the capacity decay in this study, cells with NMP solvent used for both the cathode slurry and the electrolyte still have a respectful specific capacity beyond 50 cycles (~250 mAh/g), which is equivalent to that offered by the best intercalation cathode materials known today. Finally, it should be mentioned that the observed capacity

decay is not due to dissolution of α-Li_3BN_2 into the electrolytes because we have found that the solubility of the as-synthesized α-$Li_{3-x}BN_2$ ($x > 0$) powder is less than 0.001 g in 100 mL of NMP and tetraglyme if any.

In summary, we have conducted the first-ever investigation of α-Li_3BN_2 as a transition metal free cathode material for Li-ion batteries and demonstrated a specific capacity of 890 mAh/g which is the highest specific capacity ever reported in literature for an intercalation-type cathode material. The charge storage mechanism of α-Li_3BN_2 is found to be associated with the valence state change of N ions in the BN_2 anion during Li-ion intercalation and de-intercalation. This work opens up new avenues to develop transition metal free, high capacity cathodes and lays a scientific foundation for designing high performance electrodes based on the valence state change of N ions in the future.

Acknowledgements – SE, CL, MA, KS and LS are grateful to Rowe Family Endowment Fund for Sustainable Energy. This research used resources of the Advanced Light Source, which is a DOE Office of Science User Facility under contract no. DE-AC02-05CH11231.

References

(1) J. M. Tarascon, M. Armand, *Nature* **2001**, 414, 359-367.

(2) J. B. Goodenough, Y. Kim, *Chem. Mater*. **2010**, 22, 587-603.

(3) M. S. Whittingham, *Chem. Rev*. **2004**, 104, 4271-4302.

(4) B. Kang, G. Ceder, *Nature* **2009**, 458, 190-193.

(5) A. Kraytsberg, Y. Ein-Eli, *Adv. Energy Mater*. **2012**, 2, 922-939.

(6) E.-S. Lee, A. Hug, H.-Y. Chang, A. Manthiram, *Chem. Mater*. **2012**, 24, 600-612.

(7) G. Fey, C. Lu, T. Kumar, *J. Power Sources* **2003**, 115, 332-345.

(8) C. S. Johnson, N. Li, C. Lefief, M. M. Thackeray, *Electrochem. Commun*. **2007**, 9, 787-795.

(9) J. Breger, Y. S. Meng Y. Hinuma, S. Kumar, K. Kang, Y. Shao-Horn, G. Ceder, C. P. Grey, *Chem. Mater*. **2006**, 18, 4768-4781.

(10) M. M. Thackeray, S.-H. Kang, C. S. Johnson, J. T. Vaughey, R. Benedek, S. A. Hackney, *J. Mater. Chem*. **2007**, 17**,** 3112-3125.

(11) M. D. Radin, S. Hy, M. Sina, C. Fang, H. Liu, J. Vinckeviciute, M. Zhang, M. S. Whittingham, Y. S. Meng, A. Van der Ven, *Adv. Energy Mater*. **2017**, in press, DOI: 10.1002/aenm.201602888.

(12) D. H. Seo, J. Lee, A. Urban, R. Malik, S. Y. Kang, G. Ceder, *Nature Chem.* **2016**, 8, 692-697.

(13) M. Sathiya, G. Rousse, K. Ramesha, C. P. Laisa, H. Vezin, M. T. Sougrati, M-L. Doublet, D. Foix, D. Gonbeau,W.Walker, A. S. Prakash, M. Ben Hassine, L. Dupont, J-M. Tarascon, *Nature Mater.* **2013**, 12, 827-835.

(14) K. Luo, M. R. Roberts, R. Hao, N. Guerrini, D. M. Pickup, Y.-S. Liu, K. Edström, J. Guo, A. V. Chadwick, L. C. Duda, P. G. Bruce, *Nature Chem.* **2016**, 8, 684–691.

(15) P. G. Bruce, S. A. Freunberger, L. J. Hardwick, J. M. Tarascon, *Nat. Mater*. **2012**, 11, 19-29.

(16) A. Manthiram, Y. Fu, Y. S. Su, *Acc. Chem. Res*. **2013**, 46, 1125-1134.

(17) H. Yao, G. Zheng, P.-C. Hsu, D. Kong, J. J. Cha, W. Li, Z. W. Seh, M. T. McDowell, K. Yan, Z. Liang, V. K. Narasimhan, Y. Cui, *Nat. Commun.* **2014**, 5, 3943.

(18) L. Chen, Y. Liu, M. Ashuri, C. Liu, L. Shaw, *J. Mater. Chem. A* **2014**, 2, 18026-18032.

(19) L. Chen, Y. Liu, F. Zhang, C. Liu, L. Shaw, *ACS Appl. Mater. Interfaces* **2015,** *7*, 25748-25766.

(20) K. Nemeth, *Int. J. Quantum. Chem*. **2014**, 114, 1031-1035.

(21) K. Nemeth, *J. Chem. Phys*. **2014**, 141, 054711.

(22) K. Nemeth, International Patent application PCT/US14/45402, **2016**.

(23) H. Yamane, S. Kikkawa, M. Koizumi, *J. Solid State Chem*. **1987**, 71, 1-11.

(24) F. Delnick, K. Waldrip, T. Monson, N. Dudney, L. Baggetto, G. Veith, Sandia National Laboratories Report, SAND2014-18582, **2014**.

(25) C. Koz, S. Acar, Y. Prots, P. Höhn, M. Somer, *Z. Anorg. Allg. Chem*. **2014**, 640, 279-285.

(26) Z. Zuo, Z. Xu, R. Zheng, A. Khanaki, J.-G. Zheng, J. Liu, *Sci. Rep.* **2015**, 5, 14760.

(27) Q. Wu, J.-H. Park, S. Park, S. J. Jung, H. Suh, N. Park, W. Wongwiriyapan, S. Lee, Y. H. Lee, Y. J. Song, *Sci. Rep.* **2015**, 5, 16159.

(28) S. Ishiyama, Y. Baba, R. Fujii, M. Nakamura, Y. Imahori, *Mater. Trans*. **2014**, 55, 539-542.

(29) Y. Sun, Y. Li, J. Sun, Y. Li, A. Pei, Y. Cui, *Energy Storage Mater*. **2017**, 6, 119-124.

(30) M. Kerlau, M. Marcinek, V. Srinivasan, R. M. Kostecki, *Electrochim. Acta* **2007**, 52, 5422-5429.

(31) T. Nishi, H. Nakai, A. Kita, *J. Electrochem. Soc*. **2013**, 160, A1785-A1788.

(32) T. Sasaki, C. Villevieille, Y. Takeuchi, P. Novak, *Adv. Sci*. **2015**, 2, 1500083.

(33) K. Park, B.-C. Yu, J. B. Goodenough, *Adv. Energy Mater*. **2016**, 6, 1502534.

Figures

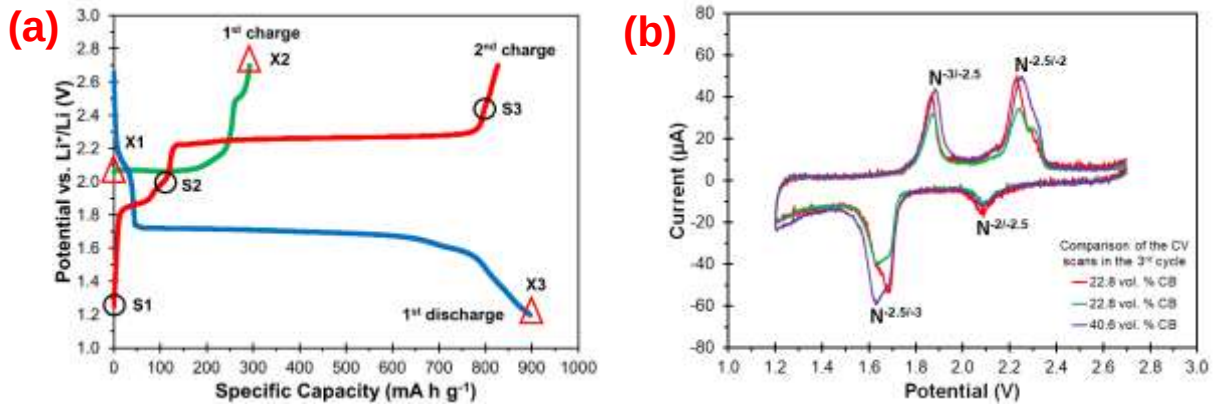

Figure 1: (a) Charge/discharge behavior of an α-Li_3BN_2 half cell at the 0.1C rate in a 2032 coin cell. Anode – Li foil; Cathode – 45 wt% CB, 10 wt% PVDF and 45 wt% α-Li_3BN_2; Electrolyte – 1M $LiCF_3SO_3$ in NMP, and (b) cyclic voltammogram of α-Li_3BN_2 half cells with a Li foil as the counter and reference electrode. Scan rate: 0.2 mA/s between 1.2 and 2.7 V. Note that cells with different CB concentrations exhibit similar CV curves.

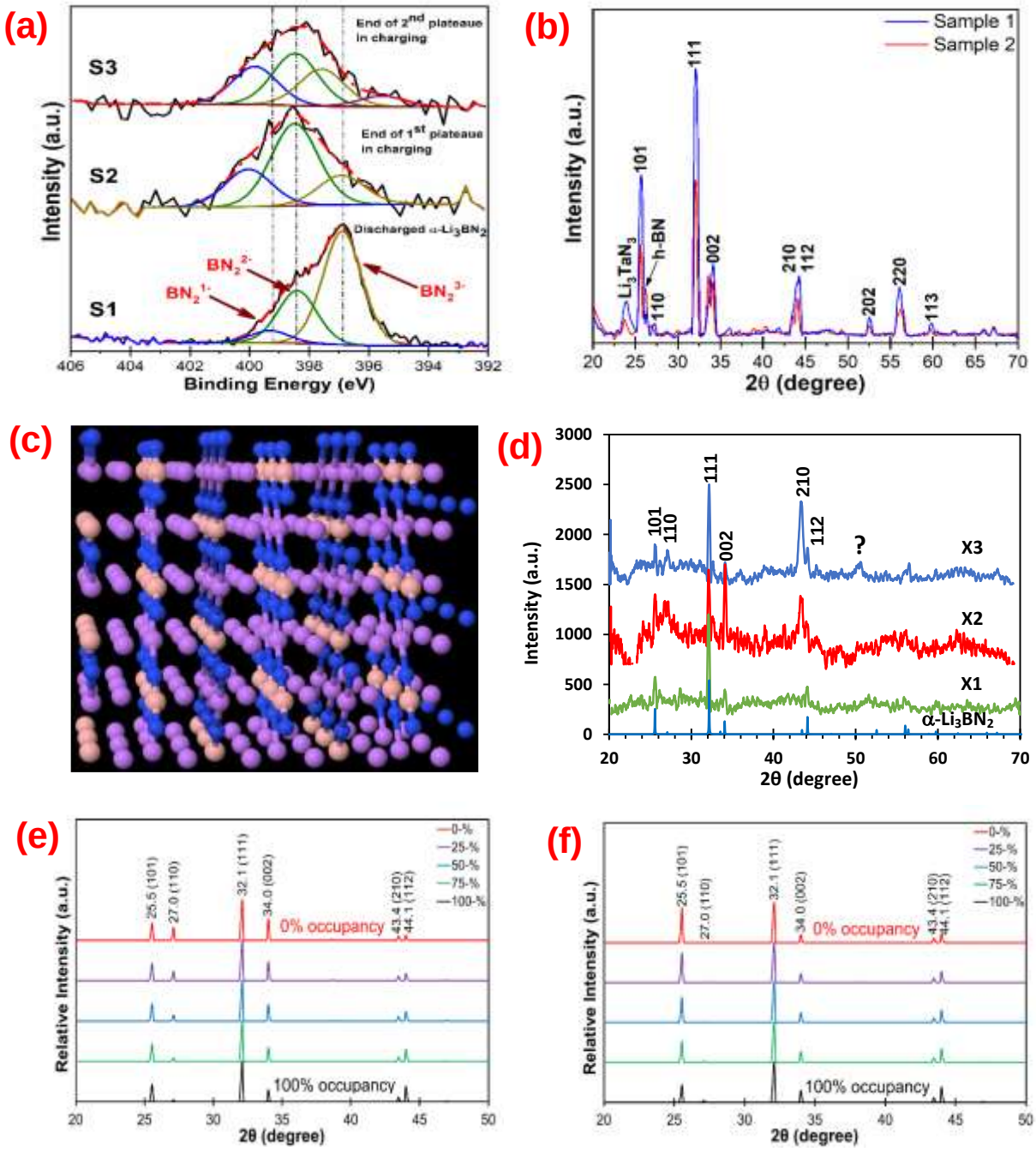

Figure 2: (a) XPS N1s spectra for the cathode at different states of charge (S1 to S3) which are indicated in Figure 1(a). **(b)** XRD patterns of the as-synthesized α-Li_3BN_2 with the peaks of α-Li_3BN_2 indexed. Sample 1 was synthesized at 900ºC and used for battery testing, while Sample 2 was synthesized at 850°C with more un-reacted BN. **(c)** The crystal structure of α-Li_3BN_2 with a 3x3x3 supercell. Color code: Li – violet, B – magenta, N – blue. There are parallel layers of -Li-N-B-N- chains and Li ions between the layers. **(d)** XRD patterns of α-Li_3BN_2 cathodes at different states of charge (X1, X2 and X3 indicated in Figure 1a) in comparison with α-Li_3BN_2 (PDF # 00-040-1166). **(e)** Modeling of changes in relative intensities of α-Li_xBN_2 peaks with respect to the site occupancy of Li ions between the layers of the linear –Li-N-B-N- chains (coordinated to 4 nearest N-s). **(f)** Modeling of changes in relative intensities of α-Li_xBN_2 peaks with respect to the site occupancy of Li ions in the layers of the linear –Li-N-B-N- chains (coordinated to 2 nearest N-s).

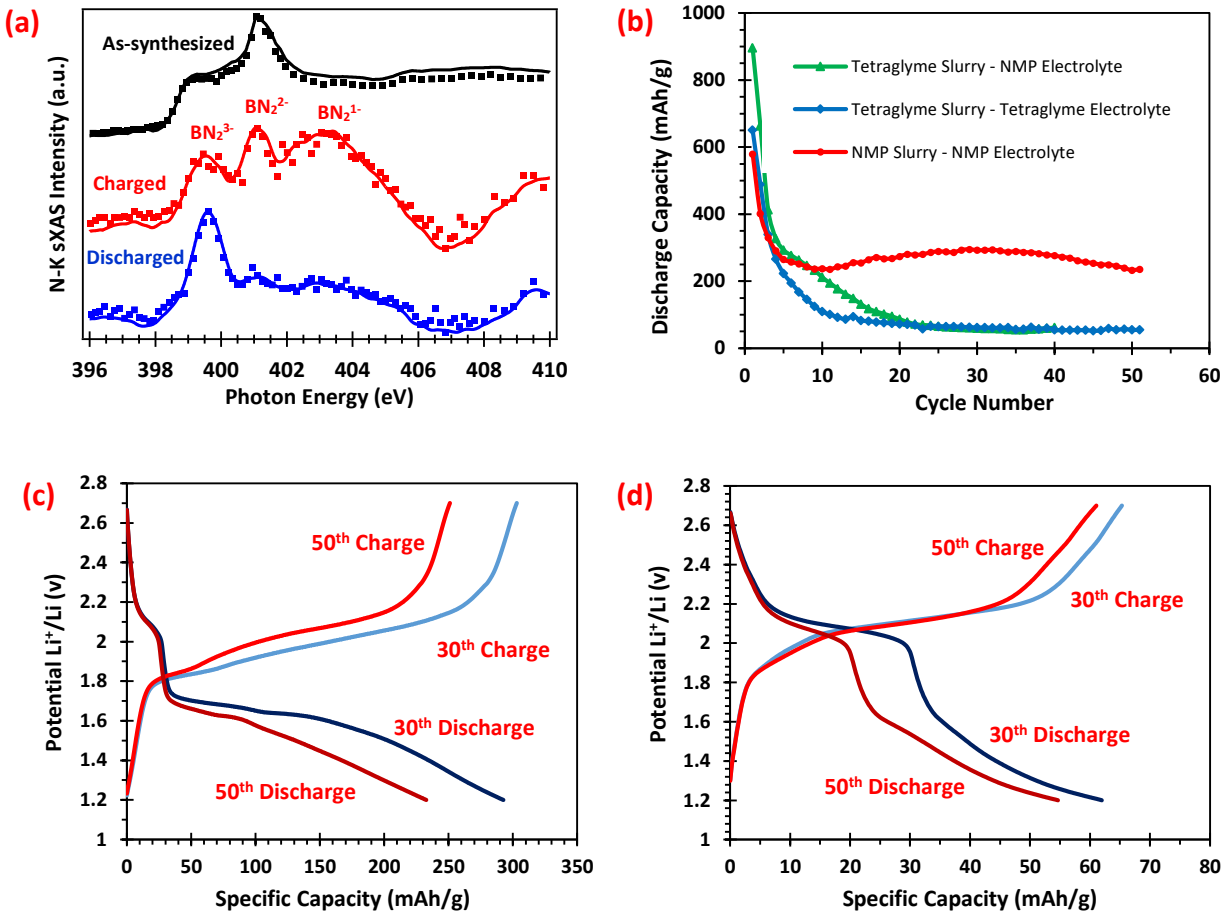

Figure 3: (a) N *K*-edge sXAS results of the as-synthesized, fully charged and fully discharged samples collected in bulk-sensitive fluorescence mode (dots – original data; solid lines – fitted curves), (b) the discharge specific capacity as a function of charge/discharge cycles for several α-Li_3BN_2 half cells prepared using NMP or tetraglyme solvent for the cathode slurry and the electrolyte as indicated, (c) the voltage profiles of the 30th and 50th charge/discharge cycles of the α-Li_3BN_2 half cell prepared using NMP solvent for both the cathode slurry and electrolyte, and (d) the voltage profiles of the 30th and 50th charge/discharge cycles of the α-Li_3BN_2 half cell prepared using tetraglyme solvent for both the cathode slurry and electrolyte.